Adsorption (2014) 20:77–89
DOI 10.1007/s10450-013-9551-2

Elasticity of adsorbent beds

Mark W. Ackley · Cem E. Celik · Kang Xu · Salil U. Rege

Received: 18 January 2013 / Accepted: 30 April 2013 / Published online: 21 May 2013

Abstract The practical application of adsorbents with the desired separation properties depends not only upon the adsorption characteristics of the material but also upon the mechanical properties of the packed bed. The packed bed, the vessel surrounding the bed and any internal structure that supports the bed are subjected to both static and cyclic loads during an adsorption process. In order to properly design the vessel and its internal structure, the bulk mechanical properties (most particularly the elastic properties) of the adsorbent bed must be known. The primary focus of this study was to determine the elastic properties of adsorbent beds packed with activated alumina, synthetic molecular sieve 13X or natural zeolite clinoptilolite. The bulk modulus of elasticity was found to be a linear function of applied stress for each of these materials in a range of stresses lower than the bulk crush strength. The Poisson's ratio for the packed bed was also deduced from these results.

Keywords Elastic properties of adsorbent beds · Bulk modulus of elasticity · Alumina · 13X zeolite · Clinoptilolite · Crush strength

M. W. Ackley (✉) · C. E. Celik (✉) · K. Xu
Praxair, Inc, 175 East Park Drive, Tonawanda, NY 14151, USA
e-mail: mark_ackley@praxair.com

C. E. Celik
e-mail: cem_celik@praxair.com

S. U. Rege
Cargill Inc, 9320 Excelsior Blvd. 164-6-9320, Hopkins, MN 55343, USA

1 Introduction

The separation capability of a porous material is of prime concern when considering either purification or bulk separation of gases by means of fixed bed adsorption processes (Ruthven 1984; Yang 1987). A considerable effort is then applied to determine the equilibrium capacity and selectivity of adsorbent materials in order to assess their potential for a desired separation. The practical application of adsorbents with the desired separation properties, however, also depends importantly upon their mechanical properties, i.e. particle properties, as well as bulk properties, of the packed bed (von Gemmingen 1994; Ackley et al. 2012). The packed bed and individual adsorbent particles are subjected to both static and cyclic loads, as are the vessel surrounding the bed and any internal structure that supports the bed. In order to properly design the vessel and its internal structure, the bulk mechanical properties of the adsorbent bed must be known. The elastic properties of the adsorbent bed are of particular interest, and the determination of these properties is the primary subject of this investigation.

2 Background

The strength of porous adsorbents and catalysts has generally been recognized with regard to resistance to attrition and crushing. Conversely, the elastic properties of the adsorbent particles and the bulk bed have received little attention. Such properties arise in the study of soil compaction and grain storage (Sawicki and Swidzinski 1995, 1998; Stasiak 2003). A common problem is the failure of steel grain storage tanks due to high stresses induced by changes in temperature (Anderson 1966; Blight 1985,

1992). Stresses that develop in the tank are not only due to thermal effects, but are also dependent upon the bulk modulus of elasticity (E) and Poisson's ratio (v) of the grain. E is a measure of the stiffness of the bed, while v is the absolute value of the ratio of the transverse strain to the axial strain. The bulk properties of the bed of granular material are different than the properties of the individual granules primarily due to the bed porosity (bed void fraction) resulting from the interparticle voids inherent in a packed bed. Friction between the particles and various particle properties no doubt affect the mechanical behavior of the bed. The chief contributors to the bed's stiffness or elasticity are the porosity of the packing and the particle modulus of elasticity. When loads are applied to the packed bed (either mechanically applied or thermally induced), the resultant stresses that develop in the vessel walls in contact with the bed are directly dependent upon the bulk modulus of elasticity of the bed. The bulk modulus of elasticity (Young's modulus) of the bed may be one or more orders of magnitude less than the individual particle modulus. Thus, it is important to determine the bulk properties of adsorbent beds for the purpose of designing the containment vessels and internal structure that support the bed. The results of this study show that the bulk modulus of elasticity of adsorbent beds is not constant but increases with increasing levels of applied stress.

The response of a packed bed of adsorbent or catalyst to applied loads depends not only upon the mechanical strength and elasticity of the particles, but also upon the packing density of the bed and the bulk crush strength (BCS). These combined properties are responsible for the elastic properties of the bed. There is usually a period of "adjustment" of the bed at the beginning of cyclic operation wherein the void fraction of the bed may decrease (compaction) due to breakage of weak particles and/or an increase in packing density resulting from the rearrangement of particles within the bed. In this study, the primary focus is on the condition where the applied or induced loads on the bed are less than the BCS, i.e. only minimal particle breakdown occurs and the bed is stable in operation. After some number of initial cycles, the forces on the bed will eventually reach a cyclic steady state. The primary interest then is determining the bulk modulus of elasticity of the adsorbent bed after it reaches a steady state condition. In order to determine this property, it is important to consider at least the initial packing density of the bed, the particle size distribution and the BCS.

The packing of the bed must reach a stable condition if the forces on the vessel, structure and bed are to achieve a cyclic steady state. The initial packing of the bed, the breakage and attrition of weak particles under load and the subsequent rearrangement of the particles in the bed induced by wall and/or supporting structure movement all affect the final (stable) packing condition of the bed. Packing the bed initially to near-maximum density minimizes the number of cycles required to achieve a stable packing. Various methods may be applied to increase the packing density beyond that resulting from simply "dumping and raking," e.g. vibration, drop-filling with distribution, rate and drop height control, etc. Gravity type filling methods have been developed for small scale devices and test fixtures as described by Gross (1949). Some of these same principles have been utilized in developing methods for loading catalysts and adsorbents in industrial scale vessels (Ackley et al. 1998; Nooy 1984; Nowobilski and Schneider 1994; Wooten 1998). Vibration, distributed filling and/or small scale gravity filling methods have been applied in the bench-scale testing of the present study.

Particle size distribution affects the packing density and thus the bed void fraction. For many fixed bed applications utilizing available commercial adsorbents or catalysts, the distribution of particle sizes is relatively narrow, i.e. the majority of the particles settle on two adjacent screens when subjected to a U.S. Sieve Series screen stack. Depending upon the method of packing as discussed above, bed void fractions are typically in the range 0.30–0.40. Such a range is consistent with a manageable pressure drop through the bed. The average size of the particles does not determine the bed void fraction. However, the size distribution is very important to the minimum void fraction that can occur. For a bidisperse mixture of spherical beads, the ratio of maximum to minimum particle diameters, i.e. of the two major fractions, must be greater than two or three before the maximum packing density is significantly impacted (German 1989). Thus the packing density and bed void fraction are influenced by both the starting particle size distribution and any change in this distribution (breakage) resulting from compaction of the bed.

Practical operation of fixed bed adsorbers or catalytic reactors must avoid loading conditions that significantly damage or destroy the adsorbent or catalyst particles. In some processes, e.g. moving bed or fluidized bed reactors, the strength and resistance to breakage of individual particles is the main concern (Couroyer et al. 2000a). Both single particle [side crushing strength (SCS)] and BCS testing methods have been employed to determine the strength of various types of materials (Couroyer et al. 2000b). While the SCS is utilized to define the single particle Young's modulus, the BCS addresses the issue of an assemblage of particles in a bed. In the latter, particles are typically loaded into a cylindrical cup and various levels of force are applied through a piston positioned at the open end of cup. After each test at progressively higher peak loads, the particles are emptied from the cup and the size distribution is measured and compared to that of the virgin material. A BCS value is then determined from the

collection of measurements as the applied load at which some limiting weight fraction of fine particles has been generated as a result of that load, e.g. 0.5–5.0 wt%. In the ASTM Standard D 7084 -04 (2004), the BCS is defined at 1.0 wt% fines.

For the reasons mentioned above, it is important to define a BCS for the materials of this study and then to determine the bulk elastic properties of a bed at applied loads less than the BCS. The same uniaxial compression test used to determine the BCS can be applied to determine the bulk modulus of elasticity as demonstrated by Sawicki and Swidzinski (1998). Both the traditional uniaxial compression (cup) and custom compression (box) configurations have been applied in this study to evaluate bulk modulus of elasticity. The initial loading step is traditionally used to define the BCS. It is in this step that bed consolidation or compaction occurs due to breakage of weak or damaged particles and due to any loose packing of the test device during its initial loading. Subsequent unloading steps are used to evaluate the elastic properties of the bed as discussed in detail below.

3 Materials and methods

3.1 Adsorbents

Three different adsorbents are used in this study: activated alumina D201 (5 × 8) and molecular sieve 13X APG II (8 × 12) supplied by UOP (Des Plaines, IL), and the natural zeolite clinoptilolite TSM140 supplied by Steelhead Specialty Minerals (Spokane, WA). The first two adsorbents are in the form of spherical beads while the TSM140 is a granular adsorbent. The characteristics of the individual materials, including the shape and smoothness of the particles, undoubtedly affect the initial compaction of the bed and the ultimate elasticity of the bed.

3.2 Test bed configurations

Two different containment devices were used for the tests. A cylindrical cup, similar to that used in BCS studies cited above, was applied in uniaxial stress measurements. A box configuration was designed to allow application and measurement of orthogonal stresses in two directions. These devices were mounted in a test machine (MTS Servo-hydraulic 20,000 lb Test Frame). The load was applied continuously through the piston. The travel of the piston was digitally controlled at a fixed rate using the servo hydraulic actuator. The piston displacement was measured by a linear variable differential transformer (LVDT) and load was measured using a load cell mounted on the axis of the piston rod.

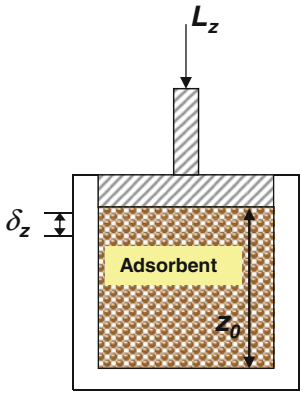

Fig. 1 Cup test device

3.2.1 *Cup tests*

The cylindrical cup (2.5 in diameter × 3.0 in deep) is illustrated in Fig. 1 along with an indication of the applied load (L_z) and bed compression (δ_z) measurement. The coordinate system used to describe stress (σ) and strain (ε) is shown in Fig. 2. The cup is loaded with adsorbent to a depth (z_0) of about two inches using a gravity filling technique similar to that described by Gross (1949). Alternatively, the adsorbent was poured into the cup and the cup was either vibrated lightly or tapped gently to pack the adsorbent. The piston travel was controlled at a rate of 0.005 in/min during both the load and unload steps. The load is applied up to some predetermined level, at which time the driving force on the piston is reversed and the bed is allowed to unload while recording both the load on the piston and its displacement.

The load/unload cycle is repeated several times for each test bed. A typical stress/displacement output from this test is shown in Fig. 3 for alumina. The initial loading produces an irreversible compaction that occurs from the breakage of weak beads and/or the additional consolidation of the bed if the cup was not fully dense-packed upon filling. Compaction in subsequent loading cycles is relatively small as evidenced by the negligible increase in the displacement between the end of the 2nd and 3rd unload cycles at near zero loading.

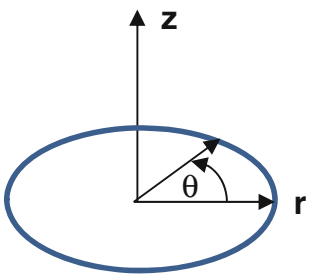

Fig. 2 Cylindrical coordinates for cup

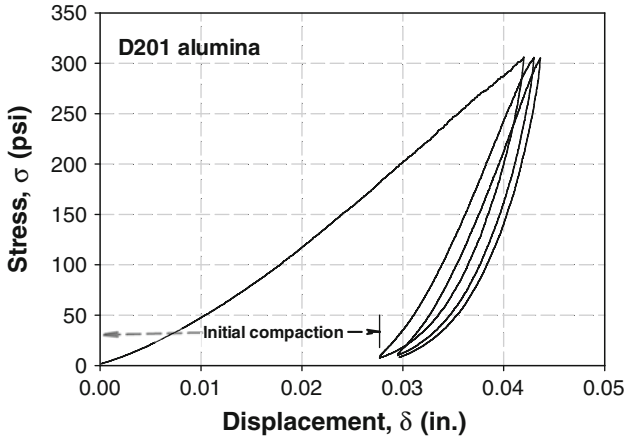

Fig. 3 Load/displacement characteristic (cup): alumina

The displacement data is converted to strain ($\frac{\delta_z}{z_0}$, in/in) and then plotted against the corresponding stress in the evaluation of modulus of elasticity. Unless otherwise noted, the stress/strain characteristics are determined from the unload part of the 3rd cycle for each test conducted. While the cup test is a convenient and simple method for evaluating bulk modulus of elasticity, lateral stresses (not measured in the above described tests) develop as a result of the complete confinement of the adsorbent bed under load. In typical adsorbers, one surface of the bed remains free to move under the influence of other applied loads on the bed. This issue is addressed through the application of the box test.

3.2.2 Box tests

The box configuration (nominally 4.0 in × 4.0 in × 4.0 in in the main chamber) is illustrated in Fig. 4 along with an indication of the applied load (L_x) and bed compression (δ_x) measurement. The primary load (L_x) is applied horizontally normal to the action of gravity. The top surface may be left completely free or a floating dead weight (L_y) may be added to simulate the silo load (Manbeck 1984) at various heights of an actual adsorber.

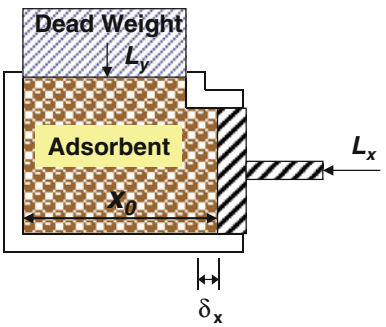

Fig. 4 Box configuration

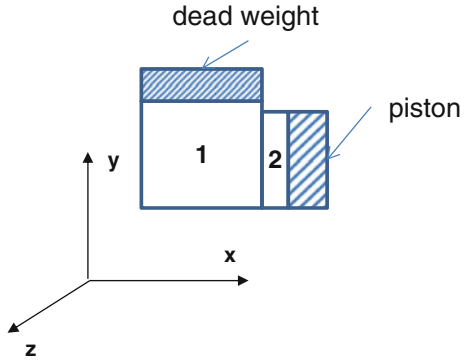

Fig. 5 Load orientation and volumes in the box

In order to prevent both the dead weight and the piston from penetrating the main adsorbent chamber, there is a small volume of adsorbent adjacent to both of these elements as illustrated in Fig. 5. The alignment of both the piston and the dead weight with the main adsorbent chamber is achieved using short guide channels machined into the sides of the box openings with mating rails in the dead weight and the piston. The dimension of the main adsorbent volume (1) shown in Fig. 5 in the x and z directions is 4.0 in, while the height (y) may vary from 4.6 in to 4.9 in depending upon the amount of adsorbent loaded. The amount of adsorbent in this main chamber (1) varied from about 74–78 in^3 for the tests in this study. Both the height (y) and depth (z) of volume (2) is 4.0 in, while the width (x) is approximately 0.45 in, resulting in an initial volume of 7.2 in^3. The piston moves within this space during the tests as loads are applied to the bed, i.e. part of the adsorbent in volume (2) is pushed into volume (1) and volume (1) expands slightly as the dead weight is pushed upward. During the loading tests, the piston face never penetrates the main chamber (1).

The box is filled and loads are applied in a manner consistent with the methods described for the cup test. The test frame was turned onto its side to accommodate this loading configuration and the piston travel was controlled at a rate of 0.1 in/min. The primary differences between this test and the cup test are the volume of adsorbent in the test device (6.5 times greater volume in the box compared to the cup), the increased rate of loading due to the reduced constraint and increased initial bed size, the quasi-free surface for expansion in one dimension and the application of the load normal to the gravitational vector. The latter two features of the box test better represent the condition of real adsorbers (circular or annular cross section) than the cup test. The dead weights used in the box test varied from 20 lb (1.25 psi) to 120 lb (7.5 psi), with this maximum stress well above the silo load developed in tall adsorbers. One limitation of the box test is that the resulting stresses are limited compared to the cup test because of the smaller load capacity of the load cell (5,000 lb) in this study.

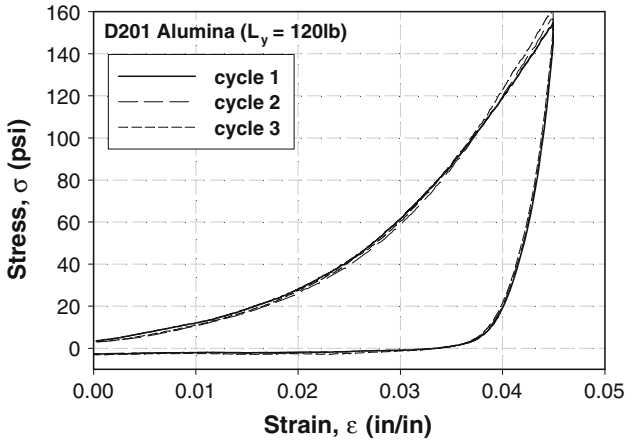

Fig. 6 Load/displacement characteristic (box): alumina ($L_y = 120$ lb)

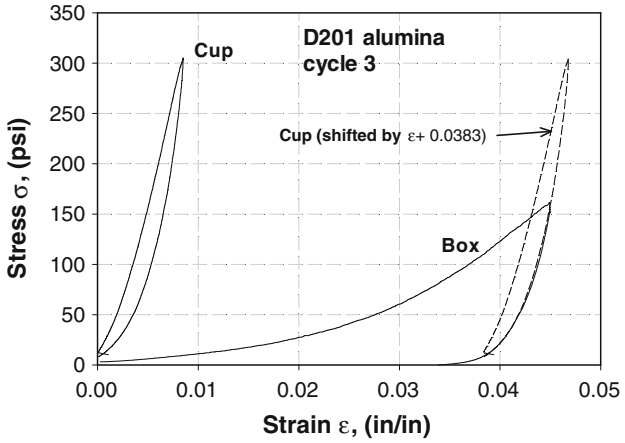

Fig. 7 Stress/strain characteristics for D201 alumina

The stress/displacement characteristics for D201 alumina in the box configuration are shown in Fig. 6. The displacement is much larger than in the cup test for an even lower maximum applied stress. There appears to be no significant compaction at this loading as the load and unload curves are completely reversible. The larger container, quasi-free surface and lower maximum load all contribute to this behavior.

When the results from the cup and box tests are compared, as in Fig. 7, the two characteristics appear to be different. However, shifting the cup characteristic along the strain axis (dashed line in Fig. 7) and overlaying the box stress/strain data shows that the unload characteristics are almost identical for stresses ≤ 150 psi.

3.3 Stress–strain relationships

3.3.1 Formulation for uniaxial compression testing (cup)

Referring to the cylindrical coordinate system shown in Fig. 2, the expressions for strain (ε) in all directions are obtained from Hooke's Law:

$$\varepsilon_r = \frac{1}{E}\left[\sigma_r - v\left(\sigma_\theta + \sigma_z\right)\right] \tag{1}$$

$$\varepsilon_\theta = \frac{1}{E}\left[\sigma_\theta - v\left(\sigma_r + \sigma_z\right)\right] \tag{2}$$

$$\varepsilon_z = \frac{1}{E}\left[\sigma_z - v\left(\sigma_r + \sigma_\theta\right)\right] \tag{3}$$

The other variables in these equations are the modulus of elasticity of the bed (E), stress (σ) and Poisson's ratio (v). The cup prevents displacement in the radial (r) direction, resulting in the following boundary conditions:

$$\varepsilon_r = \varepsilon_\theta = 0 \tag{4}$$

Applying Eq. (4) with the first three equations, rearranging and combining terms results in the simplified relationship for E:

$$E = \frac{\sigma_z}{\varepsilon_z}\left(1 - \frac{2v^2}{1 - v}\right) \tag{5}$$

An apparent modulus of elasticity (E^*) resulting from the cup test is defined:

$$E_c^* = \frac{\sigma_z}{\varepsilon_z} \tag{6}$$

E_c^* is not a constant, but varies with applied stress. Substituting Eq. (6) into Eq. (5):

$$E = E_c^*\left(1 - \frac{2v^2}{1 - v}\right) \tag{7}$$

E_c^* is determined by differentiating the measured stress/strain characteristic, i.e. approximated by calculating the slope of the unload curve at each local point (i):

$$\left(E_c^*\right)_i \approx \left(\frac{\Delta\sigma_z}{\Delta\varepsilon_z}\right)_i \tag{8}$$

The bed modulus of elasticity (E) cannot be completely defined without determining Poisson's ratio (v). One approach is to measure the radial stress (σ_r) in addition to σ_z and ε_z. In the present study, the test equipment and fixtures did not allow for the measurement of σ_r. As a result, the box test is introduced and Poisson's ratio will be deduced from the combination of cup and box test results.

3.3.2 Formulation for lateral compression with quasi-free surface (box)

Referring to the rectangular coordinate system shown in Fig. 5, the expressions for strain (ε) in all directions are obtained from Hooke's Law:

$$\varepsilon_x = \frac{1}{E}\left[\sigma_x - v\left(\sigma_y + \sigma_z\right)\right] \quad (9)$$

$$\varepsilon_y = \frac{1}{E}\left[\sigma_y - v\left(\sigma_x + \sigma_z\right)\right] \quad (10)$$

$$\varepsilon_z = \frac{1}{E}\left[\sigma_z - v\left(\sigma_x + \sigma_y\right)\right] \quad (11)$$

Bed displacement is possible in the x and y directions, but not in the z direction:

$$\varepsilon_z = 0 \quad (12)$$

Substituting Eq. (12) into Eq. (11) gives the following relationship:

$$\sigma_z = v\left(\sigma_x + \sigma_y\right) \quad (13)$$

Rearranging and combining terms results in the simplified relationship for E:

$$E = \frac{1}{\varepsilon_x}\left[\sigma_x\left(1 - v^2\right) - v\sigma_y\left(1 + v\right)\right] \quad (14)$$

The stress (σ_y) resulting from the applied dead weight is small ($\leq$7.5 psi) in comparison to the stress (σ_x) from the applied load (L_x). Thus, the second term inside the brackets in Eq. (14) is small in comparison to the first term. Simplifying Eq. (14) with this change results in:

$$E \approx \frac{\sigma_x}{\varepsilon_x}\left(1 - v^2\right) = E_b^*\left(1 - v^2\right) \quad (15)$$

The apparent modulus of elasticity (E^*) resulting from the box test is defined:

$$E_b^* = \frac{\sigma_x}{\varepsilon_x} \quad (16)$$

Similar to the cup tests, E_b^* is approximated at each local stress $(\sigma_x)_i$ by calculating the slope of the measured stress/strain characteristic:

$$\left(E_b^*\right)_i \approx \left(\frac{\Delta\sigma_x}{\Delta\varepsilon_x}\right)_i \quad (17)$$

Similarly, the bed modulus of elasticity (E) cannot be completely defined without determining Poisson's ratio (v). σ_z was not measured in the present study, so v cannot be determined directly from these data alone.

3.3.3 Reconciliation of Poisson's ratio

Apparent moduli of elasticity E_c^* and E_b^* are determined from the results of tests described as "cup" and "box" tests. However, the bed modulus of elasticity E is the desired property to use in structural calculations involving the bed. In order to determine whether or not E_c^* and/or E_b^* vary significantly from E, it is necessary to deduce the Poisson's ratio (v). While E_c^* and E_b^* may depend upon the configuration of the test, it is assumed that the bed properties E and v are independent of the test configuration. Eqs. (7) and (15) show that E^* will always be greater than E for the practical range of Poisson's ratio, i.e. $0 \leq v \leq 0.5$. The dependence of E/E^* upon v is shown in Fig. 8 for both the cup and box tests. E differs from E_c^* and/or E_b^* by 10 % or less for $v \leq 0.2$ and by 2 % or less for $v \leq 0.1$.

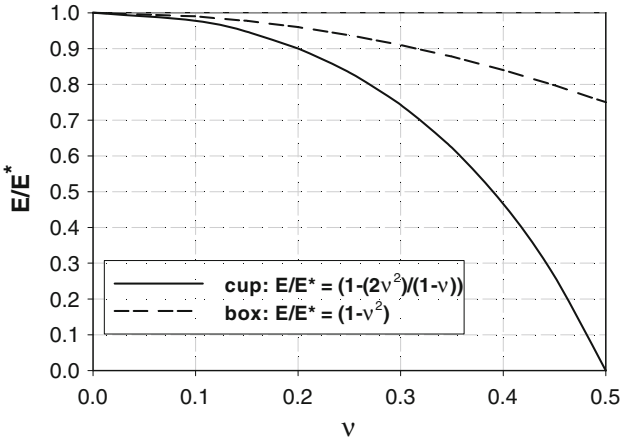

Fig. 8 Effect of Poisson's ratio on modulus of elasticity ratio

The right hand sides of Eqs. (7) and (15) are set equal to give the following:

$$E = E_c^*\left(1 - \frac{2v^2}{1 - v}\right) = E_b^*\left(1 - v^2\right) \quad (18)$$

It follows that:

$$\frac{E_b^*}{E_c^*} = \frac{\left(1 - \frac{2v^2}{1-v}\right)}{\left(1 - v^2\right)} \quad (19)$$

It then remains to determine v from Eq. (19) after determining the ratio of the apparent moduli of elasticity from the box and cup tests. This ratio is shown as a function of v in Fig. 9.

4 Results

4.1 Crush strength

As stated previously, the primary focus in this work is to determine the elastic properties of the bed in an applied stress range within which the majority of the adsorbent particles have sufficient strength to resist breakage. Such criteria are consistent with the practical and stable operation of a fixed bed process. The beds of adsorbents of this study exhibit the majority of compaction and particle

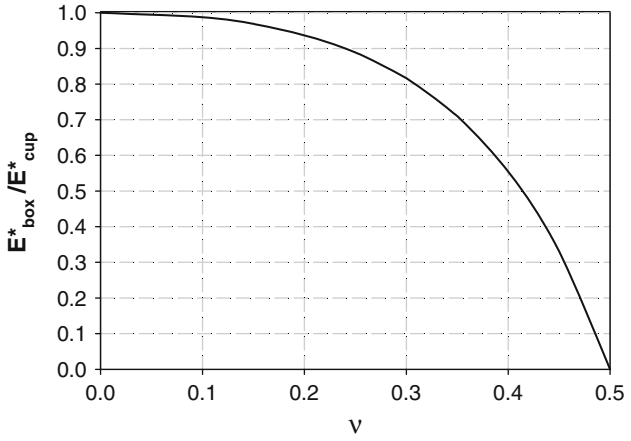

Fig. 9 Effect of Poisson's ratio on E^*_{box}/E^*_{cup}

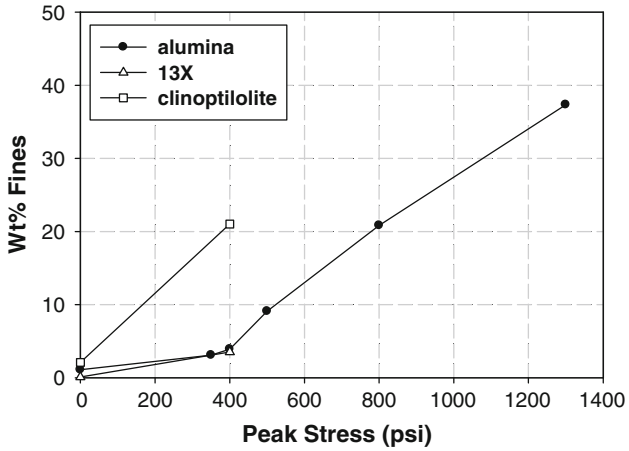

Fig. 10 Particle breakage under applied loads

breakage in the first loading cycle for applied stresses less than the BCS, with little further compaction observed in subsequent cycles. For this reason, and a matter of convenience, particle size distributions were determined after the third cycle of loading for most of the loading experiments. A shift in the particle size distribution to a smaller average particle size was observed for all three adsorbents. The effect of the applied load upon particle breakage was defined in terms of the percentage of "fine" particles generated smaller than the small end of the particle mesh size, e.g. the percentage of fines was determined for particles passing through a no. 8 screen for the 5 × 8 alumina and through a no. 12 screen for the 8 × 12 adsorbents.

Beds of D201 alumina packed in the cup configuration were subjected to peak stresses of 350, 400, 500, 800 and 1,300 psi, i.e. with three cycles of applied load at each stress level. A fresh bed was packed for each test. The percentage of fines (wt%) measured at the end of each cyclic test is compared to the original virgin adsorbent in Fig. 10. These results show a distinct effect of peak stress on breakage above a stress of about 400 psi. The percentage of fines increases from 1.1 wt% for the raw adsorbent to 3.9 wt% for the adsorbent subjected to a stress of 400 psi. Thus, 400 psi represents a reasonable BCS for this alumina.

Similar particle size measurements were performed for both 13X APG II (8 × 12) and TSM140 clinoptilolite (8 × 12) adsorbents after cyclic loading (applied peak stress of 400 psi). The results for the 13X adsorbent at 400 psi are similar to those for alumina as shown in Fig. 10. The granular and irregularly shaped clinoptilolite particles are much more susceptible to breakage at an applied stress of 400 psi. The BCS for TSM140 adsorbent is clearly well below 400 psi, although lower peak stress loading tests were not conducted for this material. Modulus of elasticity results for applied stress levels ≤400 psi are of the greatest interest in this study.

4.2 Bulk modulus of elasticity

4.2.1 Alumina

The stress/strain results from tests conducted on the alumina loaded in the cup are shown in Fig. 11 for peak stresses of 400, 800 and 1,300 psi. The 400 and 1,300 psi tests were performed with the cup loaded with virgin material. The 800 psi test was performed on the same loaded cup following the 400 psi test. The resetting of the initial displacement to zero in the 800 psi masks the residual compaction remaining in this bed at the beginning of the 800 psi test. This has no effect, however, on the evaluation of modulus of elasticity which is determined from the stress/strain unload characteristic of the 3rd cycle at this peak stress. Peak stresses well above the BCS were applied to determine the effect upon the bed elasticity.

The apparent modulus of elasticity (E^*) determined from the results in Fig. 11 is shown in Fig. 12. These results show clearly that E^* is a strong function of the applied

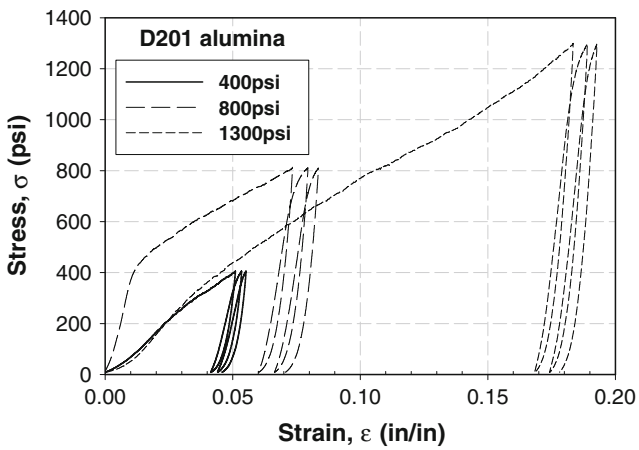

Fig. 11 Stress/strain characteristics for D201 alumina: cup

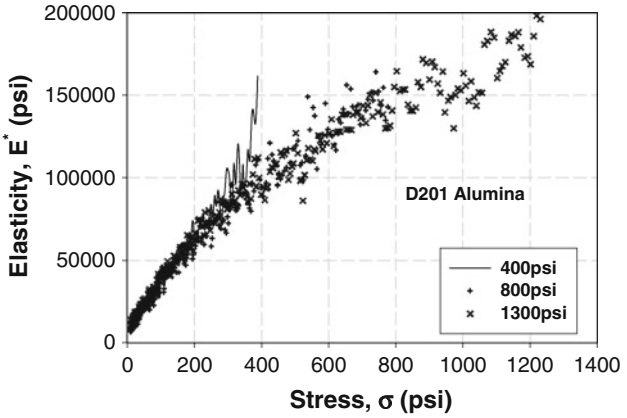

Fig. 12 Variation of apparent modulus (E^*) with stress: D201 alumina (cup)

stress, but that E^* is independent of the peak stress level in the test, e.g. E^* for applied stresses up to 400 psi is the same regardless of whether the peak stress applied was 400, 800 or 1,300 psi. The scatter in the results is likely due to particle–particle and particle–wall friction effects, as well as differentiating the relatively steep stress/strain unload characteristics. These effects are more pronounced as the stress exceeds the BCS where particle breakage continues and the bed further compacts. There is also an apparent instability in the results near the peak stress where the mode of the test changes from load to unload. The E^* results appear to be linear with applied stress up to 400 psi. Above this stress, the change in elasticity (ΔE^*) with the change in stress ($\Delta\sigma$) is less. It is reasonable to expect that E^* would tend to approach the single particle modulus as applied stress increases unbounded and the bed becomes ever more compacted as void fraction approaches a very small value. Single particle modulus of elasticity has been reported for activated alumina beads (1.7–2.0 mm catalyst support) in the range 9.0 GPa (1.3×10^6 psi)–14.5 GPa (2.1×10^6 psi) by Couroyer et al. (1999).

Tests were performed with an alumina bed packed in the box configuration shown in Figs. 4 and 5. The box was initially loaded with fresh adsorbent at a packing density of 47.5 lb/ft^3. Tests were performed with 20 and 40 lb dead weights (L_y) along with applied loads (L_x) resulting in peak stresses (σ_x) of 80 and 110 psi, respectively. Three cycles of loading and unloading were performed with each dead weight. The dead weight is displaced upward during the loading step and moves down during the unload step, although generally not returning all of the way to its initial position.

The box was re-loaded with fresh adsorbent at a packing density of 47.9 lb/ft^3. Tests were performed with 70, 100 and 120 lb dead weights (L_y) along with applied loads (L_x). Three cycles of loading and unloading were performed

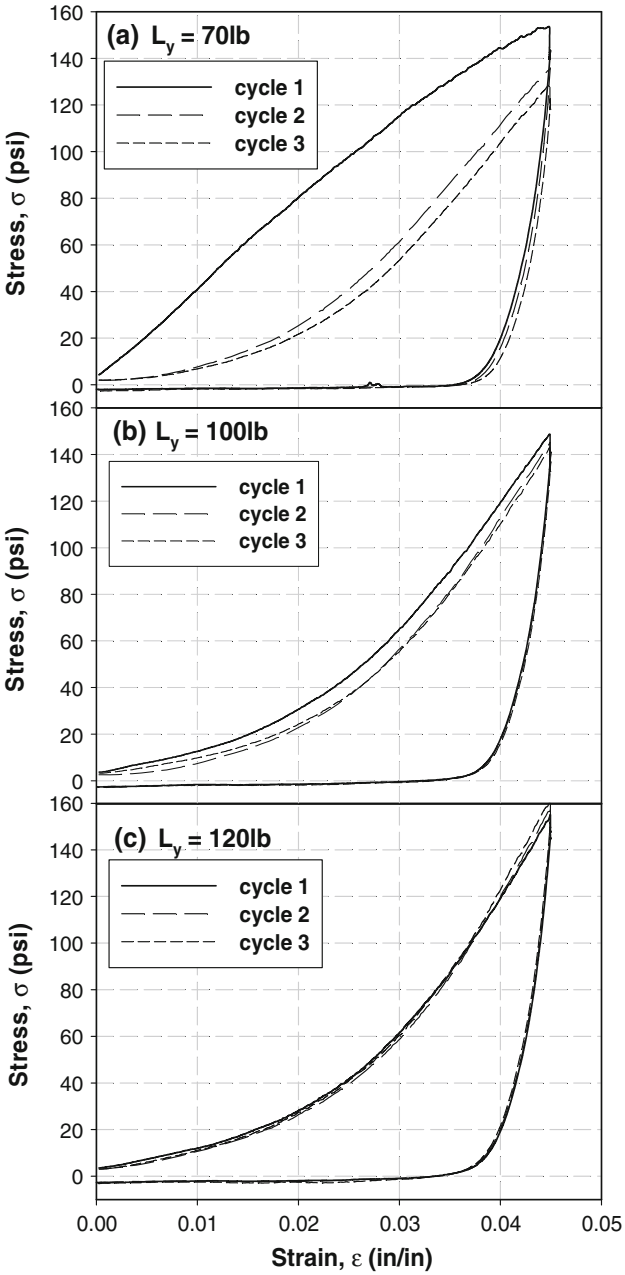

Fig. 13 Stress/strain results for D201 alumina in box tests with dead weights of **a** 70 lb, **b** 100 lb, **c** 120 lb

with each dead weight. The stress/strain characteristics for this series of tests are shown in Fig. 13. After the initial loading of the bed (70 lb dead weight), subsequent loading cycles are similar. The unload cycles within each dead weight test are almost identical and these unload characteristics are nearly indistinguishable over all three dead weight conditions. Thus, E^* is essentially the same for all dead weight conditions. The greatest bed stability is achieved after three load/unload cycles and with a dead weight $\geq$100 lb in place. A peak applied stress (σ_x) of 160 psi is obtained in combination with the 120 lb dead weight,

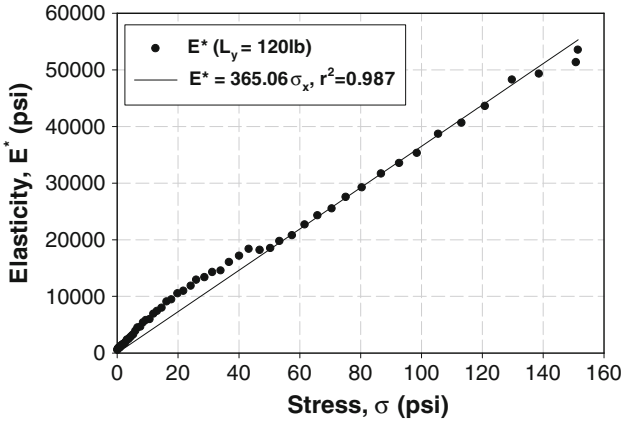

Fig. 14 Modulus of elasticity (E^*) for D201 alumina: box

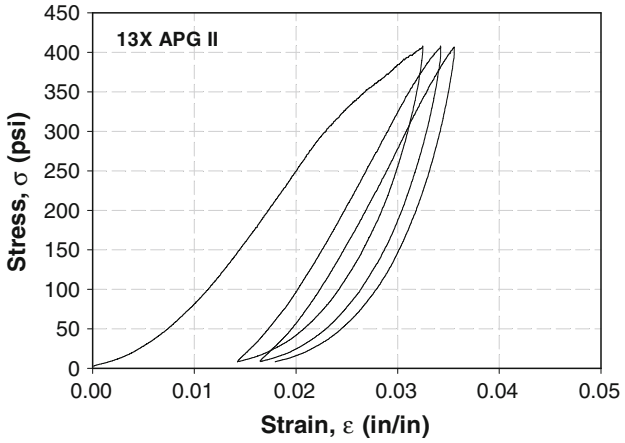

Fig. 15 Stress/strain characteristic for 13X APG II: cup

i.e. this peak stress is limited by the larger size of the box and the capacity of the load cell. The apparent modulus of elasticity (E^*) is evaluated at the most stable bed condition as shown in Fig. 14 for $L_y = 120$ lb. E^* is linear ($r^2 = 0.987$) with applied stress (σ_x) for the stress range of these data.

4.2.2 13X Molecular sieve

The cup described above was loaded with 13X APG II to a packing density of 42.6 lb/ft^3. The bed was then subjected to three cycles of loading and unloading to a peak stress (σ_z) of 300 psi. The cycling test was then repeated on the same packed bed to a peak stress of 400 psi. Crushing of beads appeared to begin at a stress of 310 psi. The packing density of the bed at the end of the six cycles was 44.3 lb/ft^3. The stress/strain results are shown in Fig. 15 for a peak stress of 400 psi.

The apparent modulus of elasticity (E^*) was determined from the unload characteristics of the third cycle of the 300 psi test and the third cycle (sixth cycle overall) of the 400 psi test. E^* is essentially linear with stress (σ_z) over the stress range of test as is evident in Fig. 16. The modulus of elasticity results are less reliable near the peak stress of a given test, e.g. as suggested by the jump in the modulus of elasticity and nonlinearity in the data around the peak stress of 300 psi shown in Fig. 16. Such behavior is not the result of the bed elasticity, but is due to the inertia of the system as the test conditions transition from loading to unloading, as well as the inherent limitation of differentiating the data near a discontinuity of this nature. The problem is avoided by extending the test to a peak stress well above the stress level of interest relative to the bulk modulus of elasticity as illustrated in the 400 psi peak stress data in Fig. 16. Box tests were not performed for 13X APG II adsorbent.

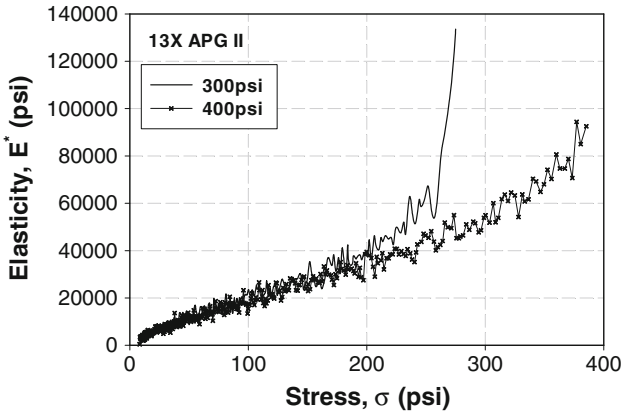

Fig. 16 Variation of apparent modulus (E^*) with stress: 13X APG II (cup)

4.2.3 Clinoptilolite

Clinoptilolite TSM140 (8 × 12, granular) was loaded into the cup to a height of 1.91 in and a packed density of 51.4 lb/ft^3. The bed was then subjected to three cycles of loading and unloading to a peak stress (σ_z) of 400 psi. The stress/strain results are shown in Fig. 17.

The apparent modulus of elasticity (E^*) was determined from the unload characteristics of the third cycle. E^* is essentially linear with stress (σ_z) over the stress range of test as is evident in Fig. 18.

Tests were performed with a clinoptilolite bed packed in the box configuration shown in Figs. 4 and 5. The box was initially loaded with fresh adsorbent at a packing density of 50.2 lb/ft^3. Tests were performed with 20 and 40 lb dead weights along with applied loads (L_x) resulting in peak stresses (σ_x) of 77 and 100 psi, respectively. Three cycles of loading and unloading were performed with each dead weight. The dead weight is displaced upward during the loading step and moves down during the unload step,

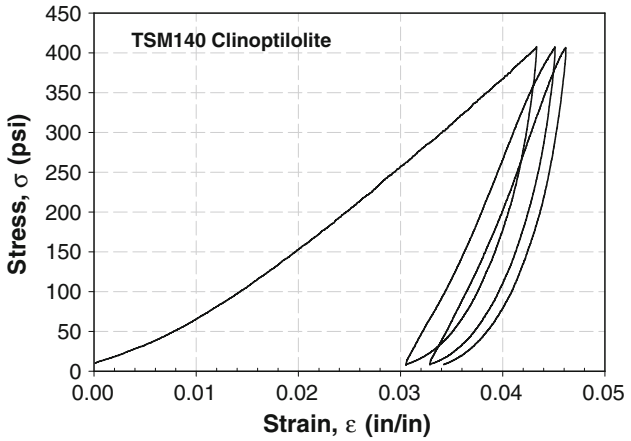

Fig. 17 Stress/strain characteristic for clinoptilolite: cup

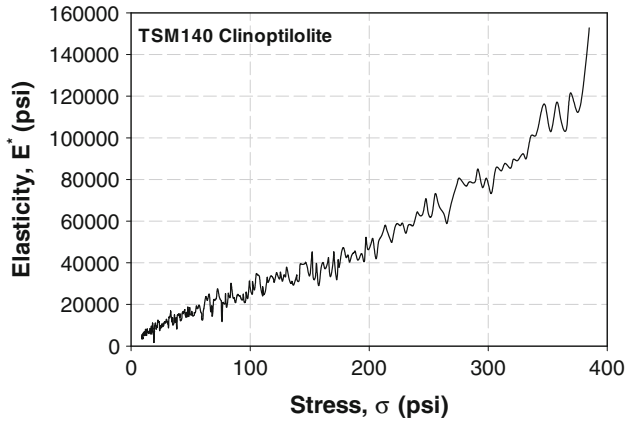

Fig. 18 Variation of apparent modulus (E^*) with stress: clinoptilolite (cup)

although generally not returning all of the way to its initial position.

The box was re-loaded with fresh adsorbent at a packing density of 49.5 lb/ft^3. Tests were performed with 70, 100 and 120 lb dead weights (L_y) along with applied loads (L_x). Three cycles of loading and unloading were performed with each dead weight. The stress/strain characteristics for this series of tests are shown in Fig. 19. The loading characteristics for each dead weight series are similar, although convergence to a single loading characteristic after nine cycles had not yet been achieved as it was with the alumina. This is presumably due to the fact that the granular clinoptilolite continued to experience some breakage. The unload cycles within each dead weight test are almost identical and these unload characteristics are nearly indistinguishable over all three dead weight conditions. A peak applied stress (σ_x) of 146 psi is obtained in combination with the 120 lb dead weight, i.e. this peak stress is limited by the larger size of the box and the capacity of the load cell.

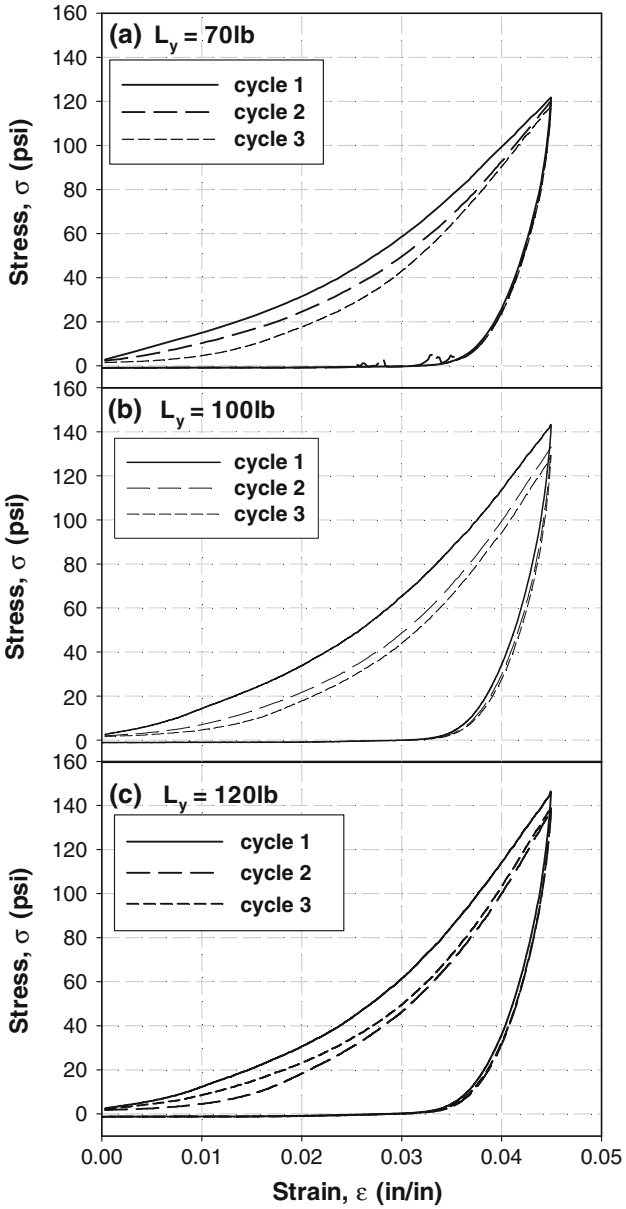

Fig. 19 Stress/strain results for TSM140 clinoptilolite in box tests with dead weights of **a** 70 lb, **b** 100 lb, **c** 120 lb

The apparent modulus of elasticity (E^*) is evaluated at the most stable bed condition as shown in Fig. 20 for $L_y = 120$ lb. E^* is linear with applied stress (σ_x) for the stress range of these data. The linear regression fit ($r^2 = 0.979$) is established for the data in the stress range 0–100 psi.

5 Discussion

In this study, the methodology of Sawicki and Swidzinski (1998) is followed with respect to determination of the bulk elastic properties of the packed bed during the unloading

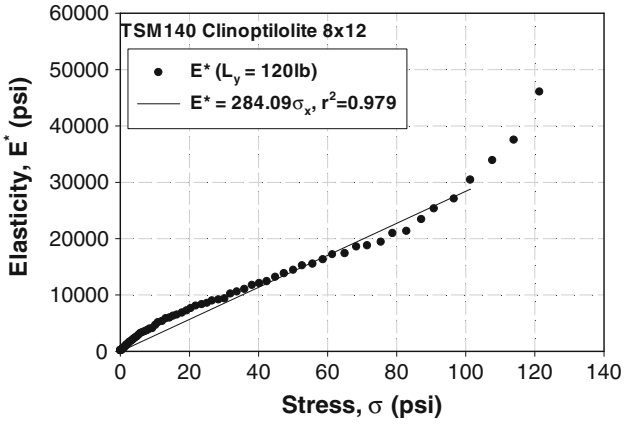

Fig. 20 Modulus of elasticity (E^*) for clinoptilolite: box

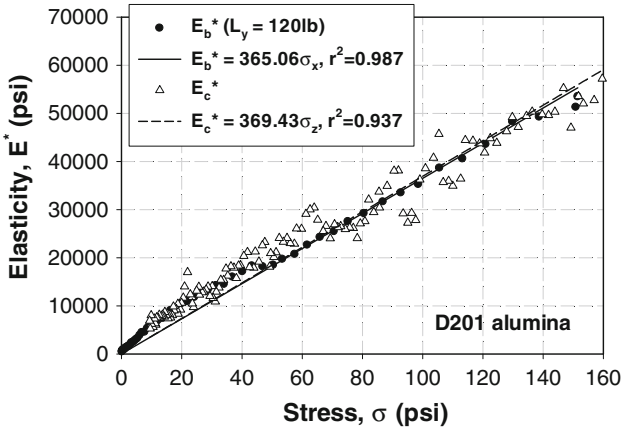

Fig. 21 Apparent modulus of elasticity compared for D201 alumina: box (E_b^*) and cup (E_c^*)

stage of stress/strain tests. Their observation that the elastic response does not depend upon the maximum level of stress applied is also consistent with the current results for adsorbents. Sawicki and Swidzinski (1998) also conclude that the elastic response is linear, i.e. the unload part of the stress/strain characteristic is elastic and can be approximated as two linear segments. This simplification leads to a constant value of the bulk modulus of elasticity, independent of stress. However, studies from soil mechanics suggest that "the dependence of elastic modulus on confining stress is supported by some theoretical consideration and dynamic testing methods" (Sawicki and Swidzinski 1998). Such a stress dependence of the bulk modulus of elasticity is also consistent with the observations of Manbeck (1984) for wheat. In the present study on adsorbents, the entire unloading response of the bed has been observed to be reversible and non-linear. As a result, the modulus of elasticity increases continuously with the level of applied stress as demonstrated in the results above for three different types of adsorbents. This result is particularly significant with respect to the structural design of the walls surrounding the adsorbent bed. The pressure exerted by the adsorbent bed on these walls is amplified (due to the increasing modulus of elasticity) under the influence of increased "squeezing" of the walls on the bed that result from induced thermal forces.

The apparent modulus of elasticity for D201 alumina obtained from the cup and box tests is compared in Fig. 21 over the applied stress range of 0–160 psi. The results from both types of tests are in close agreement. Each data set was fit linearly (zero intercept), and the respective slopes of the E^* characteristics were determined as indicated in Fig. 21. From the ratio of the slopes, $E_b^*/E_c^* = 0.9882$. It is then apparent from Fig. 9 that $\nu \approx 0.1$ and that the apparent moduli of elasticity from the cup and box tests are essentially equal. Using the value $\nu \approx 0.1$ in Fig. 8, it is evident that the actual (E) and the apparent (E^*) modulus of elasticity are also approximately equal.

The same conclusions are supported by the results for clinoptilolite shown in Fig. 22 over the applied stress range of zero to 100 psi. The results from both types of tests are in close agreement. From the ratio of the slopes, $E_b^*/E_c^* = 0.9568$. The fit to the cup data (exhibiting much more scatter) improves by including data at higher stress levels, e.g. fitting the cup data over the range 0–125 psi, the fit is improved ($r^2 = 0.846$), $E_b^*/E_c^* = 0.9883$. However, it is important to compare the cup and box test results over similar stress ranges, noting that the maximum stress is limited for the box configuration as discussed previously. Using these two ratios of apparent moduli in Fig. 9, ν values are computed as $\nu \approx 0.17$ and 0.1, respectively. This comparison shows the sensitivity of the fit to determining a final value of ν. Nevertheless, the conclusion that the apparent moduli of elasticity (E^*) from the cup and box tests and the actual modulus of elasticity (E) are all approximately equal remains reasonable for clinoptilolite.

Poisson's ratio has been addressed through the use of two different types of stress/strain measurement

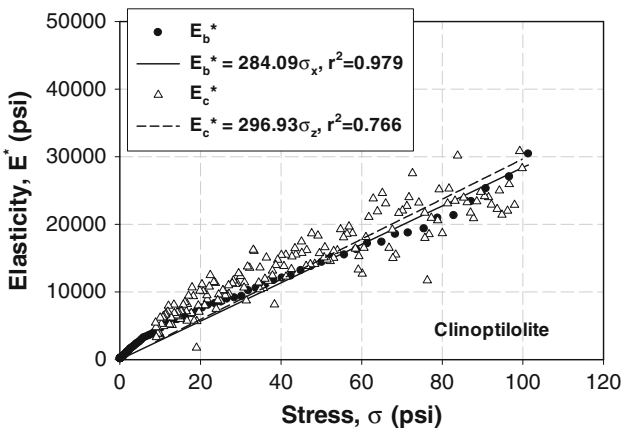

Fig. 22 Apparent modulus of elasticity compared for TSM140 clinoptilolite: box (E_b^*) and cup (E_c^*)

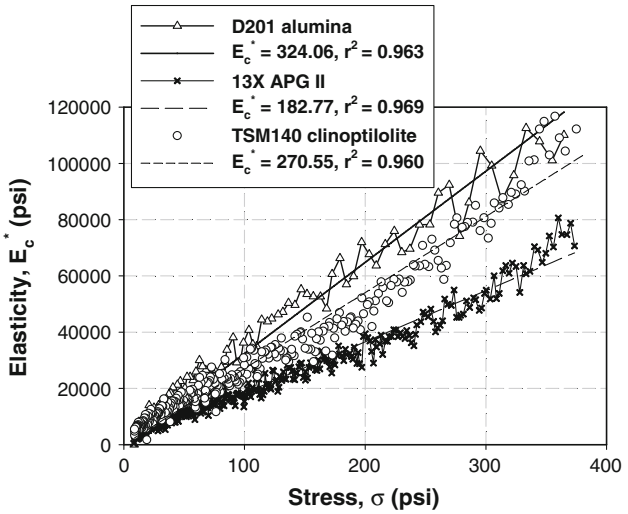

Fig. 23 Variation in modulus of elasticity with stress for beds of alumina, 13X APG II and clinoptilolite

configurations rather than attempting to measure lateral stresses and directly solve for ν. In either case, there remains a degree of uncertainty regarding this parameter. This is not uncommon, e.g. values of ν for wheat determined from experiments vary from 0.1 to 0.29, while recommendations contained in standards are as high as $\nu = 0.4$ (Molenda and Stasiak 2002). Having shown that $\nu \leq 0.2$ for the adsorbents of this study, it was further shown that ν in this range has a relatively small effect upon both E and E^*. As a result, the exact determination of ν is unnecessary for beds of these adsorbent materials. Concluding that $E \approx E_c^*$ implicitly assumes $\nu \approx 0$ and conservatively overstates E by no more than 10 % (see Fig. 8) when the true value of $\nu \leq 0.2$. The uncertainty is even less if $E \approx E_b^*$ is used.

The adsorbents of this study include both synthetic and natural zeolites, an activated alumina, spherical beads and irregular shaped granules. The modulus of elasticity for beds of these adsorbents can be determined with reasonable accuracy directly from simple stress/strain measurements using the cup configuration described above. The bulk modulus of elasticity is compared for beds of D201 alumina, 13X APG II zeolite and TSM140 clinoptilolite in Fig. 23. The bed containing alumina is the least elastic while the bed of 13X molecular sieve is the most elastic. Similar results can be obtained using the methods described above for other adsorbents.

6 Conclusions

The elastic properties of adsorbent beds packed with activated alumina, synthetic molecular sieve 13X or natural zeolite clinoptilolite have been determined for the first time. A new type of box test fixture was developed and used along with the standard cup test to measure on a small scale the stress/strain characteristics of these adsorbent beds. The apparent modulus of elasticity was determined from these results and a Poisson's ratio was deduced using the results from both types of tests in the absence of lateral stress measurements. It was found that Poisson's ratio was small enough so that the actual modulus of elasticity can be approximated well by the apparent moduli from either type of test. The bulk modulus of elasticity was found to be a linear function of applied stress for all of the materials tested in this study, i.e. for stresses less than the BCS. The simple cup test can be used to determine similar results for other adsorbents.

References

Ackley, M.W., Nowobilski, J.J., Smolarek, J., Schneider, J.S.: Multiple adsorbent loading method and apparatus for radial flow vessel. US 5,836,362 17 Nov. 1998

Ackley, M.W., Celik, C.E., Nowobilski, J.J., Schneider, J.S.: Radial flow reactor with movable supports, US 8,216,343 10 Jul. 2012

Anderson, P.F.: Temperature stresses in steel grain-storage tanks. Civ. Eng. ASCE **36**, 74 (1966)

ASTM Standard D 7084-04: Standard test method for determination of bulk crush strength of catalysts and catalyst carriers. American Society for Testing Materials (2004)

Blight, G.E.: Temperature changes affect pressures in steel bins. Int. J. Bulk Solids Storage Silos **1**, 1–7 (1985)

Blight, G.E.: Temperature-induced loading on silo walls. Struct. Eng. Rev. **4**, 61–71 (1992)

Couroyer, C., Ning, Z., Ghadiri, M., Brunard, N., Kolenda, F., Bortzmeyer, D., Laval, P.: Breakage of macroporous alumina beads under compressive loading: simulation and experimental validation. Powder Technol. **105**, 57–65 (1999)

Couroyer, C., Ghadiri, M., Laval, P., Brunard, N., Kolenda, F.: Methodology for investigating the mechanical strength of reforming catalyst beads. Oil Gas Sci. Technol.—Rev. IFP **55**, 67–85 (2000a)

Couroyer, C., Ning, Z., Ghadiri, M.: Distinct element analysis of bulk crushing: effect of particle properties and loading rate. Powder Technol. **109**, 241–254 (2000b)

German, R.M.: Particle Packing Characteristics. MPIF, Princeton (1989)

Gross, W.E.: Packing granular materials. Mech. Eng., 469-472 (1949)

Manbeck, H.B.: Predicting thermally induced pressures in grain bins. Trans. ASAE **27**, 482–486 (1984)

Molenda, M., Stasiak, M.: Determination of the elastic constants of cereal grains in a uniaxial compression test. Int. Agrophysics **16**, 61–65 (2002)

Nooy, F.M.: Dense loading. Oil Gas J., 152–157 (1984)

Nowobilski, J.J., Schneider, J.S.: Particle loader. US 5,324,159 28 Jun. 1994

Ruthven, D.M.: Principles of Adsorption and Adsorption Processes. Wiley, New York (1984)

Sawicki, A., Swidzinski, W.: Cyclic compaction of soils, grains and powders. Powder Technol. **85**, 97–104 (1995)

Sawicki, A., Swidzinski, W.: Elastic moduli of non-cohesive particulate materials. Powder Technol. **96**, 24–32 (1998)

Stasiak, M.: Determination of elastic parameters of grain with oedometric and acoustic methods. Res. Agr. Eng. **49**, 56–60 (2003)

von Gemmingen, U.: Designs of adsorptive dryers in air separation plants. Linde Rep. Sci. Technol. **54**, 8–12 (1994)

Wooten, J.T.: Dense and sock catalyst loading compared. Oil Gas J. **96**, 66–70 (1998)

Yang, R.T.: Gas Separation by Adsorption Processes. Butterworth, Stoneham, MA (1987)